

## Electron densities and temperatures in a xenon afterglow with heavy-ion excitation

G. Ribitzki, A. Ulrich, B. Busch, W. Krötz, and J. Wieser  
*Fakultät für Physik E12, Technische Universität München, D-85748 Garching, Germany*

D. E. Murnick  
*Department of Physics, Rutgers University, Newark, New Jersey 07102*  
 (Received 4 March 1994)

The time dependence of electron densities and temperatures in a heavy-ion-beam-excited gas target has been determined. A pulsed beam of 89-MeV  $^{32}\text{S}$  ions, 2-ns pulse width, was used for the excitation of xenon at pressures of 500, 1000, and 1500 hPa. This type of excitation leads to the formation of a unique afterglow plasma. Electron densities and temperatures are of the order of those found in typical low-pressure gas discharges, but the electrons, ions, and excited atoms are embedded in a cold, dense gas. Molecule formation is therefore an important process. The dissociative recombination of  $\text{Xe}_2^{+*}$  molecules, which leads to the emission of the second excimer continuum of xenon at a wavelength of 172 nm, was used as a probe at times longer than 200 ns after termination of the beam pulses. The emission of light at shorter times was modeled by solving the coupled rate equations of the collisional and radiative processes involved.

PACS number(s): 52.70.Kz, 52.40.Mj, 82.40.Ra, 52.25.Qt

### INTRODUCTION

A unique type of afterglow plasma is formed when a pulse of energetic heavy ions is stopped in a gas target. Collisions of the projectiles with target atoms lead to ionization with a high probability for multiple ionization of the target species [1–4]. The energy and angular distribution of the electrons produced in such ion-atom collisions has been the subject of detailed theoretical and experimental studies [5–7]. The subsequent excitation processes in which the electrons transfer their energy to target atoms in dense gas targets have been studied less frequently. Similar collisional cascades in solids or biological samples are the subject of a wide field of research [8]. Energy deposition by heavy ions in dense gases or plasmas are of interest for the design of gas detectors for heavy ions, in nuclear pumped lasers research [9,10], research on lasers pumped by heavy-ion beams [11,12], and heavy-ion-beam induced inertial confinement fusion studies [13,14]. A common aspect of these very different applications of heavy-ion-beam excitation is that the high energy loss  $dE/dx$  of heavy ions in matter leads to high local energy and electron densities along the primary path, although the average energy deposition can vary over many orders of magnitude.

In this paper we report on an experimental study of the time dependence of electron densities and temperatures for average energy densities of the order of  $10 \mu\text{J cm}^{-3}$  and a specific excitation power of  $4 \text{ kW cm}^{-3}$ . The results are relevant for fission fragment pumped and ion-beam pumped lasers in the infrared and visible spectral region. The study is based mainly on experimental data obtained by time resolved optical spectroscopy of the second excimer continuum of xenon. With a few plausible assumptions, the data at late times after the beam pulses can be described by a single recombination pro-

cess. Data in the early phases are analyzed by a model solving the rate equations for all the kinetic processes leading to the emission of light on the second continuum. The initial parameters for the full model are chosen in a way that the computed values match those obtained from the data for late times when only recombination is important.

### EXPERIMENT

The experiments were performed at the Munich Tandem van de Graaff accelerator. A schematic drawing of the setup is shown in Fig. 1. It consisted of a gas target which was isolated from the beamline vacuum by a  $1.3 \text{ mg/cm}^2$  titanium entrance foil for the beam and an apparatus for time resolved optical spectroscopy. A pulsed beam of 100-MeV  $^{32}\text{S}^{9+}$  ions was used. The energy loss in the entrance foil was 11 MeV. The beam pulses had 2-ns width and a repetition rate of 78 kHz. They consisted of  $5 \times 10^5$  ions per pulse which corresponds to a pulse energy of  $8 \mu\text{J}$  and an instantaneous beam power of 4 kW. The beam was focused to a diameter of 3 mm which resulted in a specific energy and power deposition of  $1.5 \text{ mJ/g}$  and  $0.8 \text{ MW/g}$ , respectively. The target remained essentially at room temperature because of the low average power deposition (1 W). Emission of light from a small volume (about  $1 \text{ mm}^3$ ) on the ion-beam axis next to the Ti entrance foil was focused with a  $\text{MgF}_2$  coated Al mirror onto the entrance slit of a vacuum ultraviolet grating monochromator. This normal incidence monochromator had a focal length of 30 cm. It was evacuated and had a  $\text{MgF}_2$  entrance window. A photomultiplier with a  $\text{MgF}_2$  window and a bi-alkali cathode was used as detector. Data were taken by photon counting, scanning the monochromator for measuring wavelength spectra and using the time to amplitude conversion (TAC)

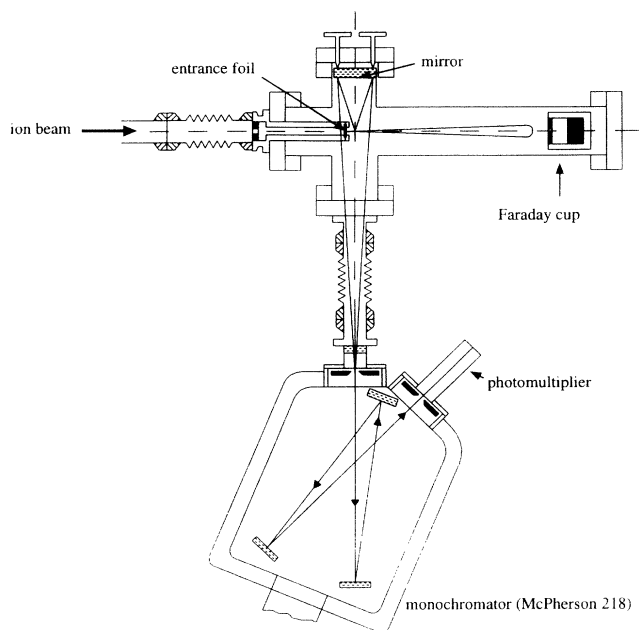


FIG. 1. Schematic drawing of the experimental setup. The ion beam enters the rare gas target through a titanium foil from the left. Light emitted from a small volume on the ion-beam axis next to the foil is focused on the entrance slit of a  $f = 30$  cm vacuum ultraviolet (vuv)-monochromator and detected with a photomultiplier.

method to obtain time spectra at a fixed wavelength. The absolute sensitivity versus wavelength had previously been calibrated.

### EXPERIMENTAL RESULTS

Time integrated spectra of rare gases near atmospheric pressure excited by heavy-ion beams are dominated by the emission from the second excimer continuum. A part of a xenon spectrum in the region of the second continuum for  $^{32}\text{S}$  beam excitation with the parameters given above is shown in Fig. 2. The continuum is centered at a wavelength of 172 nm and has a width full width at half

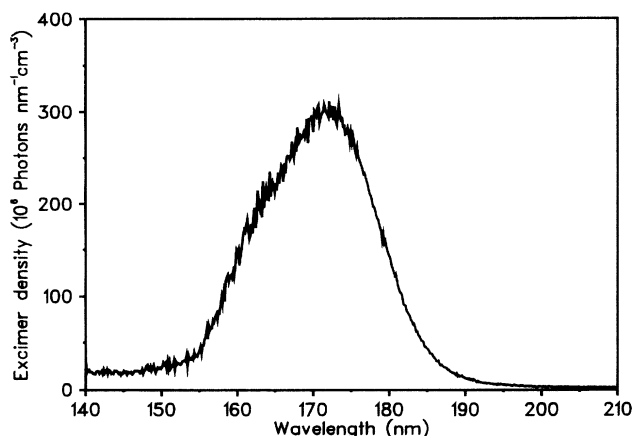


FIG. 2. Time integrated wavelength spectrum of xenon at 1000 hPa target gas pressure, excited by a pulsed  $^{32}\text{S}$  beam.

maximum (FWHM) of 15 nm. A time and wavelength integrated density of excimer molecules of  $9 \times 10^{10} \text{ cm}^{-3}$  per beam pulse at 1000 hPa target gas pressure was determined. This value is accurate to about 50%. The conversion efficiency of pulse energy of the ion beam into the second continuum excimer light is about 1%. Time spectra at a wavelength of 172 nm are shown for three different target gas pressures of 500, 1000, and 1500 hPa in Fig. 3. Note that the time scale of light emission in Fig. 3 is much longer than the 2-ns beam pulses. Therefore practically all the structure in these time spectra is due to afterglow processes in the target following excitation. A qualitative understanding of the time spectra led to the conclusion that they contain enough information to allow determination of electron density and electron temperature in the ion beam induced plasma versus time. A schematic level diagram of xenon atoms, excimer molecules, and molecular ions is shown in Fig. 4 [15]. Collisions of heavy ion projectiles with ground state xenon atoms populate the first excited levels  $^3P_1$  and  $^3P_2$  of xenon atoms, explicitly shown in Fig. 4, highly excited atomic levels ( $\text{Xe}^{**}$ ), xenon ions ( $\text{Xe}^+$ ), excited levels in xenon ions ( $\text{Xe}^{+*}$ , not shown), and multiply ionized atoms in the ground state and in excited levels ( $\text{Xe}^{n+}$  and  $\text{Xe}^{n+*}$ ,  $n > 1$ , also not shown). Free electrons are produced in the ionization processes. The species which are important for the further analysis are the  $^3P_1, ^3P_2$  resonance levels and the singly ionized atoms  $\text{Xe}^+$ . The resonance levels are populated not only by the heavy ion collisions but also by radiative and collisional cascades from  $\text{Xe}^{**}$  levels on a short time scale of about 10 ns [16]. Part of these cascades follow the "atomic side" and others form intermediate excimer molecules which rapidly decay back to form other  $\text{Xe}^*$  atoms, or finally to xenon atoms in the  $^3P_1$  and  $^3P_2$  levels:

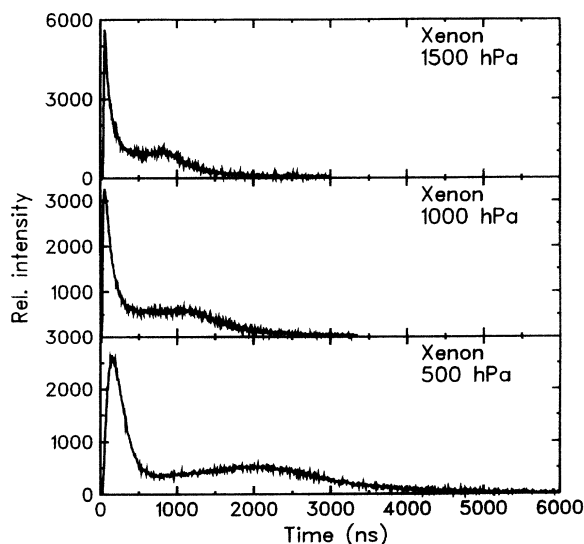


FIG. 3. Time spectra of the second excimer continuum of xenon at a wavelength of 172 nm. The beam pulses had a width of 2 ns.

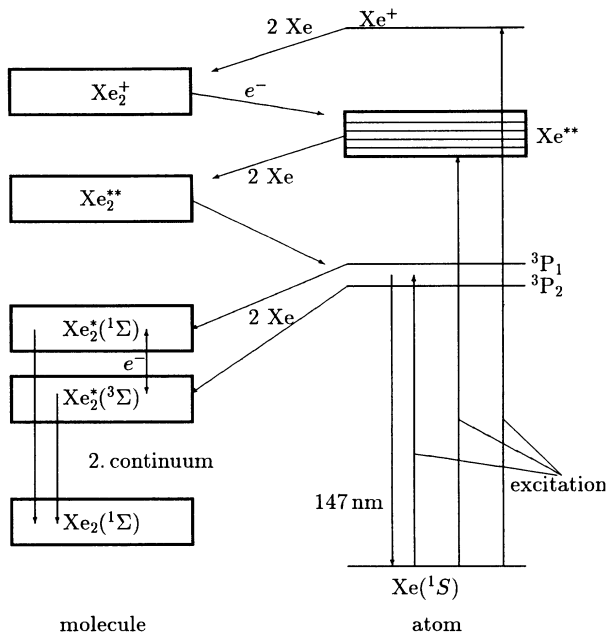
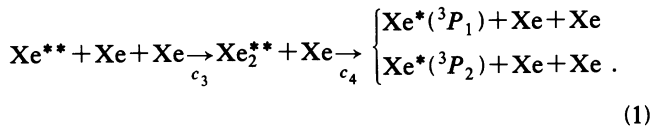
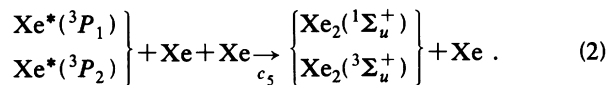


FIG. 4. Schematic drawing of the level diagram of xenon atoms (right), molecules (left) and the processes which lead to the second continuum emission.



The numerical values for the constants  $c_n$  are listed in Table I. Radiative decay of the resonance levels is slowed by radiative trapping of the resonance lines. Atoms in the  $^3P_1, ^3P_2$  levels rapidly form  $\text{Xe}^*(^1\Sigma_u^+)$  and  $^3\Sigma_u^+$  excimer molecules in three body collisions with ground state atoms with a rate constant of  $2.5 \times 10^{-32} \text{ cm}^6 \text{ s}^{-1}$  [17].

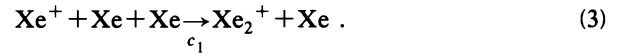


At high target densities, typically above 100 hPa, the excimer molecules relax to the lowest vibrational levels which are the upper levels of the second continuum shown in Fig. 2. Incomplete relaxation leads to another peak, the first continuum, at the short wavelength side of the second continuum close to the resonance line at 147

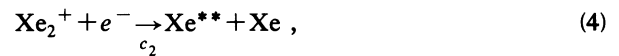
TABLE I. Rate constants for formation processes of the xenon excimer used for model calculations.

Rate constant	Value	Ref.
$c_1$	$3.5 \times 10^{-31} \text{ cm}^6 \text{ s}^{-1}$	[17]
$c_2(T)$	$2.66 \times 10^{-6} \times \left( \frac{T}{300\text{K}} \right)^{-0.6} \text{ cm}^3 \text{ s}^{-1}$	[21]
$c_3$	$3 \times 10^{-31} \text{ cm}^6 \text{ s}^{-1}$	[17]
$c_4$	$1 \times 10^{-11} \text{ cm}^3 \text{ s}^{-1}$	[17]
$c_5$	$2.5 \times 10^{-32} \text{ cm}^6 \text{ s}^{-1}$	[17]
$\tau_s$	5.5 ns	[24,25]
$\tau_t$	100 ns	[24,25]

nm. Most processes discussed so far occur on a time scale shorter than 10 ns at pressures above 500 hPa. The last step takes 40 ns at 1000 hPa. The lifetimes of the  $\text{Xe}_2(^1\Sigma_u^+)$  and  $\text{Xe}_2(^3\Sigma_u^+)$  levels are 5 and 100 ns, respectively [18]. The second continuum emission starting directly from excited atomic levels is therefore relatively fast and is the main contribution to the early, intense peak in the time spectra (Fig. 3). Excitations above the first ionization energy of xenon (12 eV) rapidly relax to form  $\text{Xe}^+$  ions. This has been confirmed for doubly ionized molecular ions formed from doubly ionized atoms in three body collisions. They decay to form singly ionized rare gas atoms emitting the so called third continuum at longer wavelengths than the second continuum [19,20]. Singly ionized atoms undergo one more rapid process in a dense target and form singly ionized molecules  $\text{Xe}_2^+$  in three body collisions with two ground state atoms with a rate constant of  $3.5 \times 10^{-31} \text{ cm}^6 \text{ s}^{-1}$  [17]:



For the electron densities discussed here the dissociative recombination of  $\text{Xe}_2^+$  molecules, which feeds back into the rapid chain forming  $\text{Xe}_2^*$  excimers, and therefore produces light on the second continuum, takes a relatively long time. The recombination rate depends on the electron temperature. Decreasing electron temperature increases the recombination rate and with it the emission of second continuum excimer light giving rise to an additional peak in the time spectra. The quantitative analysis is mainly based on the recombination rate constant and its temperature dependence measured by Shiu, Biondi, and Sipler [21]:



$$c_2(T) = c_{\text{rec}}(T) = 2.66 \times 10^{-6} \times \left( \frac{T}{T_0} \right)^{-0.6} \text{ cm}^3 \text{ s}^{-1}, \quad T_0 = 300 \text{ K} \quad (5)$$

The following reasonable assumptions were made for quantitative analysis of the data at times longer than 200 ns after termination of the beam pulses.

(a) The electrons have cooled down to room temperature at the very end of the collisional processes in the target gas.

(b) The electrons are homogeneously distributed in the observed volume.

(c) The electron density is equal to the density of molecular ions.

(d) The time scale for photon emission is dominated by dissociative recombination.

The validity of these assumptions has partly been discussed in the qualitative description of the excitation and deexcitation processes above. Losses due to transfer of excitation energy, for example, to impurities in the gas, have been minimized by using a titanium rare gas purifier in the experiments.

The differential equation for recombination is

$$\frac{dn_e}{dt} = -c_{\text{rec}} n_e n_{\text{Xe}_2^+}, \quad (6)$$

$$\frac{dn_e}{dt} = -c_{\text{rec}} n_e^2. \quad (7)$$

At the trailing slope of the light pulse the electrons are cooled to room temperature ( $T_e = 300$  K) and therefore  $c_{\text{rec}}$  has a constant value. Then Eq. (7) can be solved:

$$n_e(t) = \frac{n_{e,t=0}}{1 + n_{e,t=0} c_{\text{rec}} t}, \quad (8)$$

$$\frac{dn_e}{dt} = -\frac{c_{\text{rec}} n_{e,t=0}^2}{(1 + n_{e,t=0} c_{\text{rec}} t)^2}, \quad (9)$$

$$\frac{dn_e}{dt} = -\frac{c_{\text{rec}} n_{e,t=0}^2}{(1 + t/T_r)^2}, \quad (10)$$

$$T_r = \frac{1}{c_{\text{rec}} n_{e,t=0}}. \quad (11)$$

Taking into account that the recombination time constant  $T_r$  is much longer than the other time constants one can assume that the light intensity  $I(t)$  follows  $dn_e/dt$

$$I(t) = C \left[ -\frac{dn_e}{dt} \right] = C \frac{c_{\text{rec}} n_{e,t=0}^2}{(1 + t/T_r)^2}, \quad (12)$$

where  $C$  is a constant factor.

The analysis was started by fitting data for  $t > 2.5 \mu\text{s}$ , where  $T_e = 300$  K and therefore  $c_{\text{rec}}$  and  $T_r$  values do not depend on time. The shortest time after the beam pulse where this is still valid ( $t_0$ ) was determined by fitting Eq. (12) to the time spectra as shown in Fig. 5. This shows

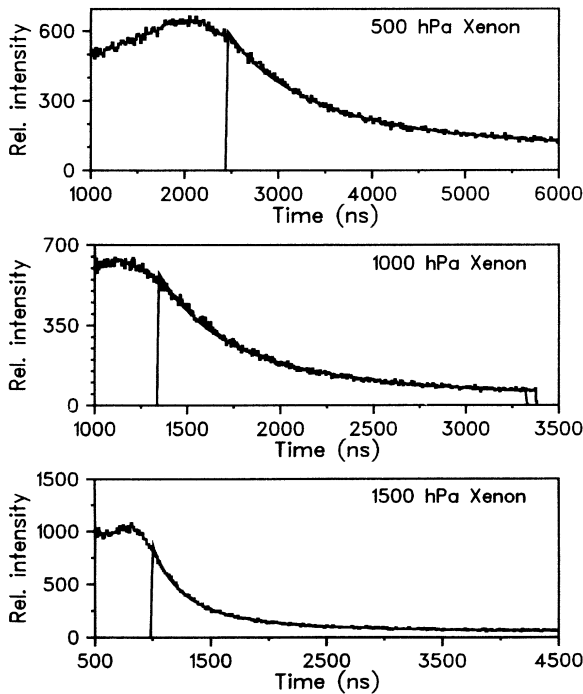


FIG. 5. Parts of the time spectra shown in Fig. 3 are shown together with fits to the data derived from the dissociative recombination of  $\text{Xe}_2^+$  molecules.

TABLE II. Electron densities after thermalization obtained by fitting Eq. (12) to the data.

Pressure (hPa)	$t_0$ (ns)	$T_r$ (ns)	$n_{e,t=0}$ ( $10^{11} \text{ cm}^{-3}$ )
500	2200	1300	3.3
1000	1200	500	8.0
1500	800	380	11.3

that the electrons are cooled to room temperature at times between 0.8 and 2.2  $\mu\text{s}$  after the beam pulses, depending on the target gas pressure. This time ( $t_0$ ), the recombination constants  $T_r$ , and electron densities  $n_e$  at time  $t_0$  are listed in Table II. In a next step, the electron density can be determined by integrating the light intensity from late times to earlier times, starting when the intensity has reached the background count rate ( $I=0$ ,  $n_e=0$ ). If assumption (d) is valid, this method to determine  $n_e(t_0)$  can be used until the processes starting at atomic levels contribute to the emission of light, about 200 ns after the beam pulses (see Fig. 3). The result is shown in Fig. 6. Electron densities between  $7 \times 10^{11}$  and  $25 \times 10^{11} \text{ cm}^{-3}$  were found at that time for the beam parameters given above. Electron temperatures can be extrapolated back to earlier times using Eq. (7), which connects the light intensity with the electron density via the recombination rate constant  $c_{\text{rec}}$ . The time dependence of  $c_{\text{rec}}$  can therefore be derived from  $I(t)$  (Fig. 3) and  $n_e(t)$  (Fig. 6). This time dependence can be used to derive the electron temperature versus time  $T(t)$  by satisfying Eq. (5). The result is shown in Fig. 7. The method can be applied until  $T_e$  is about  $12T_0$  (3600K, 0.31 eV).

Within the first 200 ns the analysis of the data requires the full set of kinetic equations leading to the formation and decay of  $\text{Xe}_2(^1\Sigma_u^+)$  and  $\text{Xe}_2(^3\Sigma_u^+)$  excimers. The rate constants of the processes which were taken into account

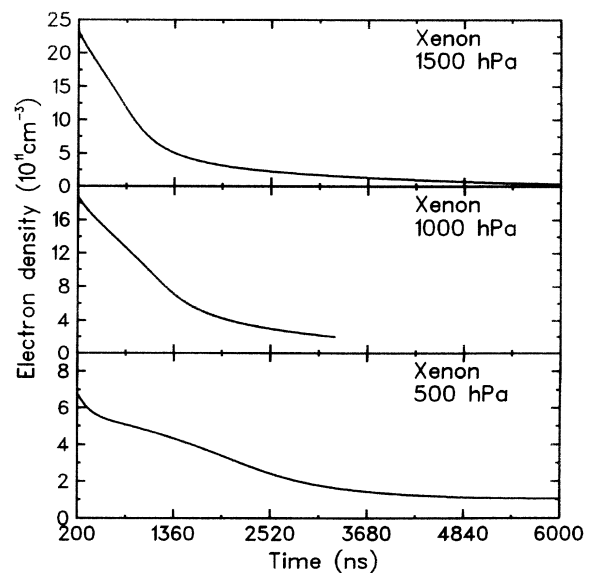


FIG. 6. Electron densities in the target gas for the pressures indicated and at times later than 200 ns after the beam pulses.

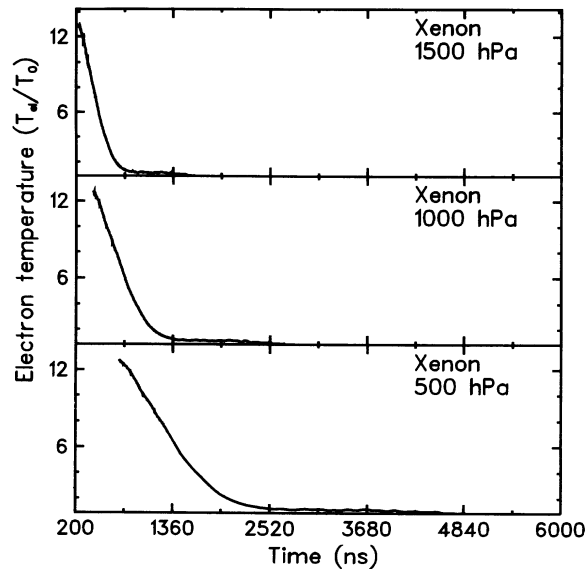


FIG. 7. Time dependence of electron temperatures. These data are calculated using the time spectra (Fig. 3) and the electron densities shown in Fig. 6.

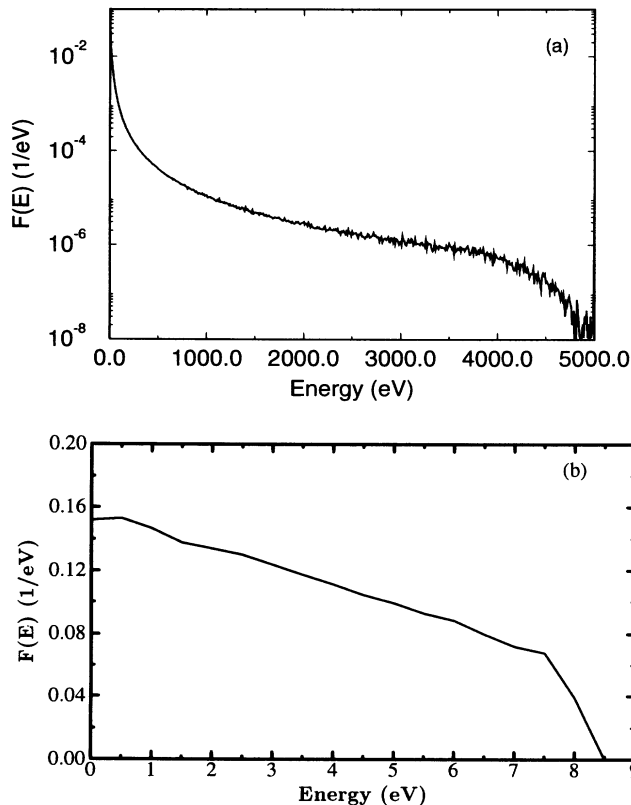


FIG. 8. Electron energy distributions calculated with a "Monte Carlo" simulation for 89-MeV  $^{32}\text{S}$ -xenon collisions: The spectrum (a) shows the initial electron energy distribution. The spectrum (b) shows the electron energy distribution when the inelastic collisions of the electrons have been traced until their kinetic energy was below the excitation threshold. The average electron energy is about 4 eV. The spectra are normalized so that  $\int F(E)dE=1$ .

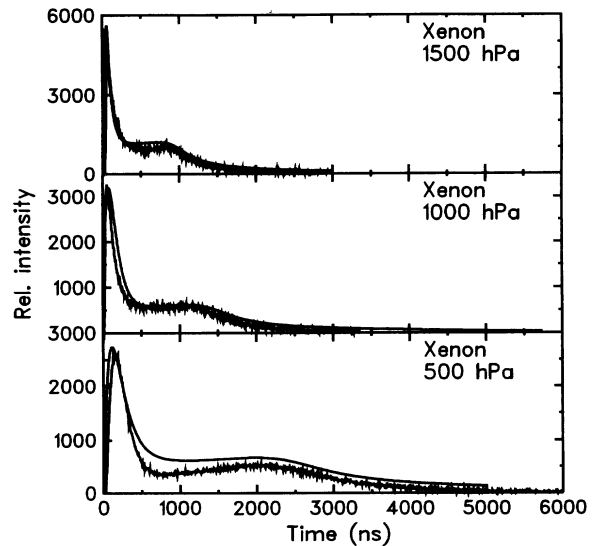


FIG. 9. Comparison of measured time spectra and time spectra calculated with the model (solid lines).

are listed in Table I. The rate equations have been numerically solved with the initial electron density and the density of excited xenon atoms as free parameters. They were adjusted so that the model reproduced the two peaks in the time spectra, the electron density determining the second peak and the density of excited xenon atoms determining the first peak. The electron temperature which is necessary to model the dissociative recombination in the first 200 ns after the beam pulses was determined to  $T_e(\text{initial})=160T_0 (=4\text{ eV})$  at a time immediately after the beam pulses. This value was calculated using a "Monte Carlo" simulation to model the initial electron energy distribution function and its time development due to inelastic collisions of the electrons in the target. The results are shown in Fig. 8. The time scale in which the initial energy distribution function [Fig. 8(a)] is changed into the energy distribution function where the electron energy is too low for further excitations of xenon atoms [Fig. 8(b)] is short compared with the pulse width of the ion beam. The first two nanoseconds in which the beam is on and the excitation and ionization processes occur are not explicitly treated in the model described here. The time dependence of the electron temperature from between the  $160T_0$  at  $t=0$  and the  $12T_0$  at  $t=200$  ns was calculated from momentum transfer cross section from literature [22]. A comparison between the time spectra (Fig. 3) and time spectra calculated with the numerical model is shown in Fig. 9. The model provides, for example, densities of excimer molecules in the xenon target separated with respect to their process of formation. This is shown in Fig. 10 for a target gas pressure of 1000 hPa.

## SUMMARY

Electron densities and temperatures have been studied in the afterglow of short pulses of a heavy-ion beam used for the excitation of dense xenon gas. High quality time

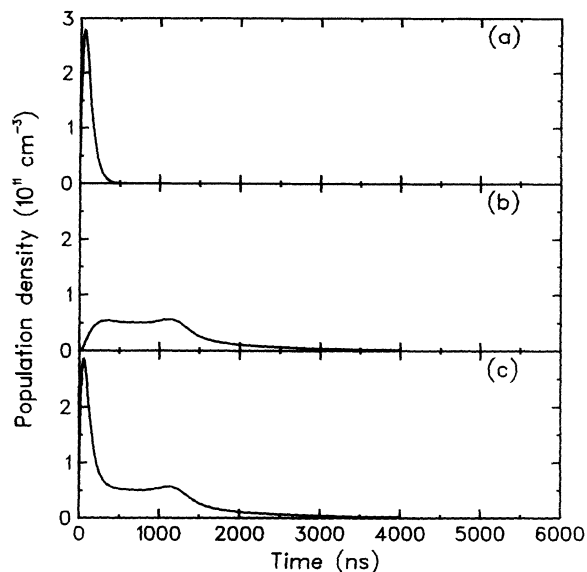


FIG. 10. Excimer densities obtained from a numeric model calculation. Data in (a) show those excimers which are formed from excited atoms and data in (b) those which are formed by dissociative recombination. The sum of both is shown in (c).

spectra were measured covering a long time interval of several microseconds after the nanosecond beam pulses. The excimer formation which is accompanied by the emission of second continuum radiation is a very efficient process under these conditions.

For an energy deposition of 1.5 mJ/g by 89-MeV  $^{32}\text{S}$  ions the density of free electrons is  $2 \times 10^{12} \text{ cm}^{-3}$  and the electron temperature 4 eV, immediately after the beam pulses. Two hundred nanoseconds later  $n_e(t)$  and  $T_e(t)$  could be determined from the time spectra which were reproduced by using the dissociative recombination of  $\text{Xe}_2^+$  molecules as the only important process for describing the time dependent emission of light. The intermediate time was described by a kinetic model. This analysis could also be applied for other rare gases and it would be interesting to perform similar studies in rare gas mixtures and other gas targets excited by heavy ion beams. The model which has been developed can be used, for example, to calculate time spectra in xenon for different excitation conditions. As the analysis was performed for an energy deposition which was determined

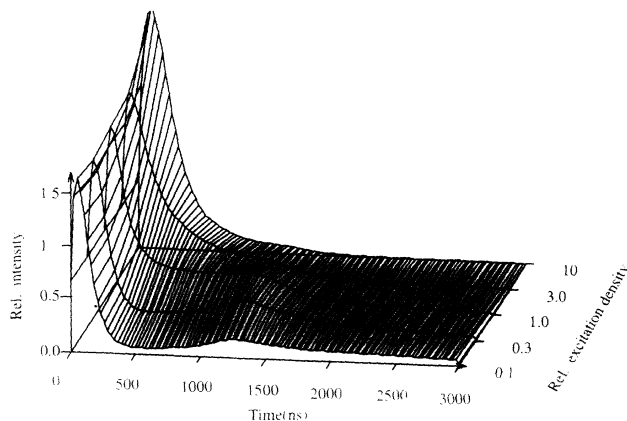


FIG. 11. Time spectra calculated for short-pulse-heavy-ion-beam excitation of a 1000 hPa xenon target for different excitation energies normalized to the excitation energy used in the experiments described in this paper.

by the power of the pulsed  $^{32}\text{S}$  beam from the Munich Tandem van de Graaff accelerator Fig. 11 shows time spectra which have been calculated for 0.1, 0.3, 3, and 10 times this energy deposition, for comparison. A lower limit of energy densities for applying this method might be reached when diffusion processes dominate over the recombination and an upper limit when the target is substantially heated and thermal ionization has to be taken into account. Finally it is interesting to note that Fig. 11 shows that the second peak in the time spectrum, which had stimulated the studies merges into the first peak at around three times the energy deposition of the experiments described here due to higher electron densities speeding up to the recombination process.

The model described here can, for example, be used for studies on excimer lasers pumped by ion beams. Such experiments have recently been described by Busch and co-workers [23].

#### ACKNOWLEDGMENT

This work has been funded by the German Federal Ministry for Research and Technology (BMFT) under Contract No. 06 TM 310 I, Gesellschaft für Schwerionenforschung GSI Darmstadt, the Tandem Accelerator Laboratory Munich, and NATO.

- [1] C. L. Cocke, *Phys. Rev. A* **20**, 749 (1979).
- [2] R. E. Olson, *J. Phys. B* **12**, 1843 (1979).
- [3] S. Kelbch, J. Ullrich, R. Mann, P. Richard, and H. Schmidt-Böcking, *J. Phys. B* **18**, 323 (1985).
- [4] S. Kelbch, J. Ullrich, W. Rauch, and H. Schmidt-Böcking *et al.*, *J. Phys. B* **19**, L47 (1986).
- [5] N. Stolterfoht, D. Schneider, D. Burch, H. Wieman, and J. S. Risley, *Phys. Rev. Lett.* **33**, 59 (1974).
- [6] Steven T. Manson, L. H. Toburen, D. H. Madison, and N. Stolterfoht, *Phys. Rev. A* **12**, 60 (1975).
- [7] L. H. Toburen, in *High Energy Ion-Atom Collisions*,

Proceedings of the International Seminar on High Energy Ion-Atom Collision Processes, Debrecen, Hungary, 1981, edited by D. Bereny (Elsevier, New York, 1982).

- [8] R. Spohr, *Ion Tracks and Microtechnology* (Vieweg, Braunschweig, 1990).
- [9] *Proceedings on the Physics of Nuclear Induced Plasmas and Problems of Nuclear Pumped Lasers, Obninsk, Russia, 1992*, edited by P. P. Dyachenko and A. V. Zrodnikov; parts of the proceedings are published as special issues of *Laser Particle Beams* [**11** (3) (1993)] and *Hyperfine Interactions* [**88** (4) (1994)].

- [10] A. Ulrich et al., *Laser Part. Beams* **11**, 505 (1993).
- [11] A. Ulrich, *J. Appl. Phys.* **63**, 2206 (1988).
- [12] T. J. Moratz, T. D. Saunders, and M. J. Kushner, *J. Appl. Phys.* **64**, 3799 (1988).
- [13] R. C. Arnold and J. Meyer ter Vehn, *Z. Phys. D* **9**, 65 (1988).
- [14] J. Meyer ter Vehn, *Nucl. Instrum. Methods A* **278**, 25 (1989).
- [15] M. McCusker, in *Excimer Lasers*, edited by Ch. Rhodes (Springer-Verlag, Berlin, 1984).
- [16] D. C. Lorentz, *Physica C* **82**, 19 (1976).
- [17] C. Duzy and J. Boness, *IEEE J. Quantum Electron.* **QE-16**, 640 (1980).
- [18] J. W. Keto, R. E. Gleason, Jr., T. D. Bonifield, and G. K. Walters, *Chem. Phys. Lett.* **42**, 125 (1976).
- [19] H. Langhoff, *Opt. Commun.* **68**, 31 (1988).
- [20] W. Krötz, A. Ulrich, B. Busch, G. Ribitzki, and J. Wieser, *Appl. Phys. Lett.* **55**, 2265 (1989).
- [21] Y.-J. Shiu, M. A. Biondi, and D. P. Sipler, *Phys. Rev. A* **15**, 494 (1977).
- [22] A. Mozumder, *J. Chem. Phys.* **11**, 6289 (1980).
- [23] B. Busch, A. Ulrich, W. Krötz, G. Ribitzki, and J. Wieser, *J. Appl. Phys.* **74**, 5960 (1993).
- [24] J. W. Keto, R. E. Gleason, Jr., and G. K. Walters, *Phys. Rev. Lett.* **33**, 1365 (1974).
- [25] D. Haaks, *Habilitationschrift*, Universität Wuppertal, 1976 (unpublished).